The Contributions to the Explosive Growth of $PM_{2.5}$ Mass due to Aerosols-Radiation Feedback and Further Decrease in Turbulent Diffusion during a Red-alert Heavy Haze in Jing-Jin-Ji in China

Hong Wang[1,2 *], Yue Peng[1,2], Xiaoye Zhang[1,3*], Hongli Liu[1], Meng Zhang[4], Huizheng Che[1], Yanli Cheng[1], Yu Zheng[1,2]

Author list:
Hong Wang, wangh@cma.gov.cn,
Yue Peng, 1131509950@qq.com; nuist_PY@163.com
Xiaoye Zhang, xiaoye@cma.gov.cn
Hongli Liu, liuhl@cma.gov.cn
Meng Zhang, 316398453@qq.com
Huizheng Che, chehz@cma.gov.cn
Yanli Cheng, chengyl@cma.gov.cn
Yu Zheng, hblfzhengyu@126.com

The Contributions to the Explosive Growth of $PM_{2.5}$ Mass due to Aerosols-Radiation Feedback and Further Decrease in Turbulent Diffusion during a Red-alert Heavy Haze in Jing-Jin-Ji in China

Hong Wang[1,2 *], Yue Peng[1,2], Xiaoye Zhang[1,3*], Hongli Liu[1], Meng Zhang[4], Huizheng Che[1], Yanli Cheng[1], Yu Zheng[1,2]

1 State Key Laboratory of Severe Weather (LASW), Chinese Academy of Meteorological Sciences (CAMS), CMA, Beijing 100081, China

2 Collaborative Innovation Center on Forecast and Evaluation of Meteorological Disasters, Nanjing University of Information Science & Technology, Nanjing 210044, China

3 Center for Excellence in Regional Atmospheric Environment, Institute of Urban Environment, Chinese Academy of Sciences (CAS), Xiamen 361021, China

4 Beijing Meteorological Bureau, Beijing 100089, China

Correspondence to: Hong Wang (wangh@cma.gov.cn), Xiaoye Zhang (xiaoye@ cma.gov.cn)

Abstract. The explosive growth of $PM_{2.5}$ mass usually results in extreme $PM_{2.5}$ levels and severe haze pollution in East China, and is generally underestimated by current atmospheric chemistry models. Based on one such model, GRPAES_CUACE, three sensitivity experiments – a "background" experiment (EXP1), "online aerosol feedback" experiment (EXP2), and an "80% decrease in turbulent diffusion coefficient" of chemical tracers" experiment, based on EXP2 (EXP3) – were designed to study the contributions of aerosol–radiation feedback (AF) and decrease in turbulent diffusion coefficient to the explosive growth of $PM_{2.5}$ during a "red-alert" heavy haze event in China's Jing–Jin–Ji region. The results showed that the turbulent diffusion coefficient calculated by EXP1 was about 60–70 m^2/s on the clear day and 30–35 m^2/s on the haze day. This difference in diffusion coefficient was not enough to distinguish between the unstable atmosphere on the clear day and extremely stable atmosphere during the $PM_{2.5}$ explosive growth stage. Also, the inversion calculated by EXP1 was obviously weaker than the actual inversion from sounding observations on the haze day. This led to a 40%–51% underestimation of $PM_{2.5}$ by EXP1; AF reduced by about 43%–57% diffusion coefficient during the $PM_{2.5}$ explosive growth stage, which strengthened the local inversion obviously; plus, the local inversion indicated by EXP2 was much closer to the sounding

observations than that by EXP1. This resulted in a 20%–25% reduction of $PM_{2.5}$ negative errors in the model, reaching as low as −16% to −11% in EXP2. However, the inversion produced by EXP2 was still weaker than the actual observation, and AF could not solve all the problems of $PM_{2.5}$ underestimation. Based on EXP2, the 80% decrease in turbulent diffusion coefficient of chemical tracers in EXP3 resulted in near-zero turbulent diffusion, referred to as an "turbulent intermittence" atmospheric state, which resulted in a further 14%–20% reduction in $PM_{2.5}$ underestimation, and the negative $PM_{2.5}$ errors were reduced to −11% to 2%. The combined effects of AF and decrease in turbulent diffusion coefficient solved over 79% of the underestimation of the explosive growth of $PM_{2.5}$ in this study. The results show that online calculation of AF is essential for the prediction of $PM_{2.5}$ explosive growth and peaks during severe haze in China's Jing–Jin–Ji region. Besides, an improving in the planetary boundary layer scheme with respect to extremely stable atmospheric stratification is also essential for a reasonable description of local "turbulent intermittence" and a more accurate prediction of $PM_{2.5}$ explosive growth during severe haze in in this region of China.

Keywords: aerosol–radiation feedback; turbulent diffusion; planetary boundary layer scheme; temperature inversion; $PM_{2.5}$

1 Introduction

Since 2013, East China has been experiencing unprecedented intrusions of severe haze accompanied by high levels of particulate matter (PM) of less than 2.5 microns in aerodynamic diameter ($PM_{2.5}$), causing wide public concern (Ding et al., 2013; Wang et al. 2013; Huang et al., 2014; Wang et al., 2014; Sun et al., 2014; Hua et al., 2016; Yang et al., 2015; Zhong et al., 2017, 2018a, 2018b). The instantaneous $PM_{2.5}$ concentration is usually in the hundreds of ug/m^3 during severe haze episodes, occasionally exceeding one thousand, in the metropolitan region of Beijing–Tianjin–Hebei, referred to here as Jing–Jin–Ji, and its surroundings of East Shanxi, West Shandong, and North Henan in East China (Wang et al., 2014; Quan et al., 2014; Sun et al., 2014; Yang et al., 2015; Zheng et al., 2016). Studies have shown, however, that models generally underestimate the explosive growth and peak values of $PM_{2.5}$ during severe hazes, especially in Jing–Jin–Ji (Wang et al., 2013; Wang et al., 2014; Li et al., 2016).

The causes of $PM_{2.5}$ explosive growth and its underestimation by atmospheric chemistry models are complex and uncertain at present, but it possibly involves local emissions, reginal transportation, aerosol physicochemical processes, gas–particle conversion, meteorological conditions, and so on. However, the actual atmospheric stability and how accurate it is described by atmospheric models is a fundamental problem that cannot be ignored among others. Local or regional meteorological conditions dictate whether haze occurs and what the $PM_{2.5}$ level may be (Zhang et al., 2014; Zheng et al., 2015; Gao et al., 2016) when source emissions are unchanged for a short period of time. The meteorological conditions of the planetary boundary layer (PBL) are a key and direct trigger for the emergence of a haze event (Wang et al., 2014; Li et al., 2016; Zhong et al., 2017). Turbulent diffusion is an important factor to characterize PBL meteorology when the atmosphere is stable. Also, it is a major pathway of particle and gaseous pollutant exchange from the surface to upper atmosphere; and when haze occurs, pollutant dispersal via the upper-level winds can take place when haze is accompanied by calm surface winds and weak vertical motion of air in surface layers and the PBL. The intensity of turbulent diffusion largely determines the severity of haze pollution. Thus, a reasonable description of turbulent diffusion by PBL schemes in atmospheric chemistry models is vital for the prediction of severe pollution (Hong et al., 2006; Wang et al., 2015; Hu et al., 2012, 2013a, 2013b; Li et al., 2016). The latest studies in this field of research show (Wang et al., 2015; Li et al., 2016) that current PBL schemes may be insufficient for describing the extremely weak turbulent diffusion

conditions when extremely severe haze occurs in Jing–Jin–Ji, which more broadly may be one important reason why $PM_{2.5}$ peaks are underestimated by atmospheric chemistry models. More specifically, there may be two independent reasons why the description of extremely weak turbulent diffusion in atmospheric models is deficient. One is that aerosol–radiation feedback (AF) is not calculated online in the model run. AF may restrain turbulence by cooling the surface and PBL while heating the atmosphere above it when aerosols with certain absorption characteristics are concentrated in the PBL (Wang et al., 2010; Forkel et al., 2012; Gao et al., 2014, 2015; Wang et al., 2015; Ding et al., 2016; Li et al., 2016; Miao et al., 2016; Petaja et al., 2016; Gao et al., 2017; Qiu et al., 2017; Zhong et al., 2018). Ignoring AF is likely to lead to an obvious overestimation of turbulent diffusion when the $PM_{2.5}$ concentration exceeds a certain value, which is worthy of further study. The other possible reason is that the extremely weak turbulence resulting in extremely severe haze is not fully described by the atmospheric chemistry model (Li et al., 2016).

In the present work, a "red-alert" heavy haze event (issued by China's Ministry of Environmental Protection when the air pollution index is forecast to exceed 300 over the next three days) that occurred during 15–23 December 2016 in China's Jing–Jin–Ji region was selected to study the contributing factors to $PM_{2.5}$ explosive growth and peaks, and the possible deficiency of atmospheric models in describing extremely weak turbulent diffusion.

2 Model, data and methods

2.1 Model

Focusing on dust and haze pollution in China and East Asia, the Chinese Unified Atmospheric Chemistry Environment (CUACE) (Gong and Zhang, 2008) was online-integrated into the mesoscale version of the Global/Regional Assimilation and PrEdiction System (GRAPES_meso), developed by the Chinese Academy of Meteorological Sciences (Chen et. al., 2008; Zhang and Shen, 2008), to build an online chemical weather forecasting model, GRAPES_CUACE (Wang et al., 2009, 2010; 2015a; Zhou et al., 2012). The main components of GRAPES_CAUCE include: a model dynamic core; a modularized physics package (Xu et al., 2008); an atmospheric chemistry module, CUCAE, with online coupling of direct and indirect aerosol feedback; and an emissions inventory. The dynamic framework of GRAPES_CUACE is semi-implicit, semi-Lagrangian, fully compressible, and non-hydrostatic (Yang et al.,

2007, 2008; Chen et al., 2008). A height-based terrain-following coordinate system is used, and there are 33 vertical layers form the surface to 30 km. A longitude–latitude grid is adopted in the spatial discretization of the model and the horizontal resolution may vary upon request. The physics package can also be tailored by the user (Xu et al., 2008), and Table 1 lists the specific physics and chemistry schemes used in this study. The gas-phase chemistry of RAD II (Stockwell et al., 1990), with 63 gaseous species through 21 photochemical reactions and 121 gas-phase reactions, is used in this study. The aerosols include sea salt (SS), sand/dust (SD), black carbon (BC), organic carbon (OC), sulfates (SFs), nitrates (NI) and ammonium salts (AM), and aerosol processes involving hygroscopic growth, coagulation, nucleation, condensation, dry and wet deposition, scavenging, aerosol activation, and so on. The formation of SF aerosols and secondary organic aerosols from gases, NI and ammonium formed through gaseous oxidation, and ISORROPIA (Fountoukis et al., 2007) calculating the thermodynamic equilibrium between NI and ammonium and their gas precursors, are considered in CAUCE, which has been evaluated and introduced in previous studies (Gong and Zhang et al., 2008; Zhou et al., 2008, 2012).

Based on the modeled aerosol concentrations, vertical profiles of temperature change, including direct aerosol impacts, are calculated by the radiation model and fed back online to the model dynamic core at each grid point and every time step, which reforms the model temperature field, dynamic process, regional circulation and meteorological conditions, in turn ultimately impacting the aerosol concentration. The external mixing of aerosols species (SS, SD, BC, OC, SF, NI, AM) and particle size bins are used in the calculation of AF, as introduced and evaluated in detail in previous studies (Wang et al., 2009, 2010, 2015a, 2015b). With this two-way GRAPES_CUACE model, aerosol–radiation–PBL–meteorological interactions, as well as aerosol–cloud–precipitation interactions and regional pollution and transportation of $PM_{2.5}$ etc., have been successfully studied (Wang et al., 2010, 2015a, 2015b; Zhou et al., 2012, 2016; Jiang et al., 2015; Zhang et al., 2018).

The turbulent diffusion coefficient is calculated by the YonSei University PBL scheme (Hong et al., 2006), which is a revised vertical diffusion package based on the nonlocal boundary layer vertical diffusion scheme in a medium-range forecast (MRF) model (Hong et al., 1996). The major ingredient of the revision is the inclusion of an explicit treatment of entrainment processes at the top of the PBL, compared with the

MRF PBL scheme. The specific calculation method of diffusion coefficient is shown in Hong et al. (1996), and has been selected as a standard option in MRF models (Caplan et al. 1997; Farfán and Zehnder, 2001; Basu, et al., 2002; Bright and Mullen, 2002; Mass et al., 2002) as well as the Weather Research and Forecasting model (Hong et al., 2006) in the National Centers for Environmental Prediction (NCEP) since its establishment.

The horizontal resolution of the model adopted here was 0.15° × 0.15°, to match the resolution of the emission source. Considering the impacts of the interregional transport of pollutants, East China (100°–140°E, 20°–60°N) (Figure 1a) was set as the model domain, but our discussion focuses mainly on the most polluted area, Jing–Jin–Ji (red frame in Figure 1a), for which Figure 1b illustrates the geographical and topographical features. There are two balloon sounding stations, Xingtai and Beijing (yellow stars in Figure 1b) in our study area. Xingtai, located in southern Hebei province at the eastern foot of the Taihang Mountains, is influenced by descending airflow from the mountains in winter, and in recent years has frequently been ranked the most polluted city in China. The topography of Xingtai and the serious haze pollution it experiences are closely related to its situation on the southern plain of Jing–Jin–Ji. Beijing, located next to Tianjin and surrounded by Hebei, lies in the transitional zone from the Yan Mountains to its southern plain, and represents the most polluted areas in the central part of Jing–Jin–Ji.

2.2 Emissions inventory

Based on the Multi-resolution Emissions Inventory for China in 2012 (He et al., 2012), the changes in East China of five kinds of emission sources – industrial, domestic, agricultural, natural, and traffic – were obtained from national statistical data with respect to industry, energy consumption, road networks, and motor vehicles, and updated to 2015 and 2016. Five reactive gases (SO_2, NO, NO_2, CO, NH_3), 20 volatile organic compounds [VOCs (ALD, CH_4, CSL, ETH, HC_3, HC_5, HC_8, HCHO, ISOP, KET, NR, OL_2, OLE, OLI, OLT, ORA_2, PAR, TERPB, TOL, XYL), listed in Table 2], and five aerosol species (BC, OC, SF, NI and fugitive dust), were obtained via the above emissions data according to the input requirement of the CUACE model. The horizontal grid resolution was 0.15° × 0.15° and there was one emissions dataset for each month at hourly intervals.

2.3 Data

Hourly observational $PM_{2.5}$ concentration data for more than 1440 surface observational stations (blue dots in Figure 1) from the China National Environmental Monitoring Centre (http://www.cnemc.cn) during 15–23 December 2016 were used to evaluate the model results. The hourly observational meteorological data, including wind speed and temperature, from 500 surface automatic observation stations of the China Meteorological Administration (CMA) in the Jing–Jin–Ji region (red triangle in Figure 1b), were used for model validation. Meteorological balloon sounding data from the CMA at 0000 UTC (early morning) and 1200 UTC (dusk, local time) in Beijing and Xingtai (yellow star in Figure 1b) during the same period were also used to compare with the modeled results. There is one AERONET station (Holben et al., 1998), Xianghe, and two CARSNET stations (Che et al., 2009; 2014; 2015), Beijing and Shijiazhuang, in the Jing–Jin–Ji region (black crosses in Figure 1b). Observed aerosol optical depth (AOD) and single scattering albedo (SSA) data from these three stations during the same period were also used for model evaluation. NCEP 0.25° × 0.25° global analysis gridded data (https://rda.ucar.edu/datasets/ds083.3) were used as the model's initial and six-hourly lateral boundary meteorological input fields. The initial values of chemical tracers were obtained according to their five-year mean climatic values. The results of the first 120 hours of the model were discarded to eliminate the effects of the chemical initial fields.

2.4 Experimental design

Both dynamic processes of the regional atmosphere and solar radiation have important impacts on turbulent diffusion and PBL processes. When severe haze occurs, it has been showed from observation study (Zhong et al., 2018) that surface-level daily direct radiative exposure is reduced by around 89% compared with clean days, suggesting the possibility of a huge difference in turbulent diffusion between severe haze and clean days. However, it is difficult to distinguish between the two reasons for extremely weak turbulent diffusion in the true atmosphere, because of the complicated relationship between atmospheric dynamics and solar radiation. However, meaningful results might be possible by conducting sensitivity experiments using an atmospheric chemistry model. Here, three such experiments (EXP1, EXP2, and EXP3 – see Table 3 for descriptions) were designed to discuss the contributing factors to extremely weak turbulence and corresponding $PM_{2.5}$ explosive growth, along with the insufficient description of extremely weak turbulent diffusion by PBL schemes in atmospheric chemistry models. All other model

dynamic processes, physical options, and initial input data of the meteorology and chemical tracers were same for the three experiments, i.e., except the differences shown in Table 3. In EXP3, a further decrease in the turbulent diffusion coefficient based on EXP2 was only applied to the diffusion coefficient of chemical tracers in CUACE mode; the diffusion coefficient in other physical packages and the dynamic framework of GRAPES_MESO was the same as in EXP1 and EXP2.

3 Results and discussion

The studied haze episode began on 15 December 2016. $PM_{2.5}$ began to gather and climb slowly at this time, but was below 150 ug/m^3 in most of Jing–Jin–Ji from 00:00 UTC 15 to 00:00 UTC 17 December – a period we refer to as the "climbing stage" of $PM_{2.5}$. From 00:00 UTC 17 to 00:00 UTC 21 December, $PM_{2.5}$ increased rapidly, and reaching a peak of 400–600 ug/m^3 in most of the study area. We refer to this period as the "explosive growth stage" of $PM_{2.5}$. In this section, we focus mainly on the contributions of AF and decrease in turbulent diffusion coefficient to the $PM_{2.5}$ during this stage.

3.1 Synoptic background

The circulation in the upper atmosphere and the surface-level synoptic system controlling Jing–Jin–Ji remained relatively stable during the maintenance of this haze episode. Figure 2 displays the geopotential height, temperature, and winds in the upper (500 hPa), middle (700 hPa) and lower (850 hPa) atmosphere, as well as PBL levels (900, 950, 1000 hPa), at 0000 UTC 19 December 2016, to show the meteorological background. It can be seen that the geopotential height in the upper atmosphere (500 hPa) showed zonal circulation in East Asia. There was a horizontal trough north of Jing–Jin–Ji (black frame) in the upper and middle atmosphere (500 and 700 hPa), and the region was controlled by moderate northwesterly or westerly air flow at the bottom of the trough. The temperature and wind fields at 500 and 700 hPa both showed that cold air in the upper and middle atmosphere was weak. The 850-hPa geopotential height showed that the subtropical high in the East Sea was strong; also, Jing–Jin–Ji was in the pressure equalization field to the northwest periphery of the subtropical high and the wind was very weak at this level due to the blocking of the subtropical high. The 900-, 950- and 100-hPa geopotential heights all showed that Jing–Jin–Ji was located in the pressure equalization field between the "northwest land high" and southeast subtropical high within the whole PBL, and the land high was weaker than the subtropical

high. This resulted in a small pressure gradient, weak and thin wind fields, and a stable atmospheric situation within the PBL, which was conducive to the maintenance of the haze episode.

3.2 Observation–model comparison

Meteorological factors not only at the surface but also in the PBL are key in affecting haze processes and $PM_{2.5}$ concentrations (Wang et al., 2014a, 2014b). Unfortunately, however, most numerical models struggle to simulate these aspects, which is also a key point determining the performance of atmospheric chemistry models (Hu et al., 2013a, 2013b; Li et al., 2016).

Using hourly meteorological data from surface automatic observation stations of the CMA, the surface wind speed and temperature at Beijing and Xingtai, and the average for Jing–Jin–Ji, according to the results of EXP1, EXP2 and EXP3, were evaluated for the period 15–24 December 2016 (Figure 3). It can be seen that, in Beijing, the modeled surface wind speed in the three experiments was in good agreement with observation, in terms of the overall trend as well as the maximum and minimum values. The observed and modeled wind speed was basically below 2 m/s during 17–21 December (i.e., the explosive growth stage of $PM_{2.5}$). The modeled wind speed at Xingtai was slightly worse than that at Beijing, but the overall trend of change was basically consistent with observation, and the wind speed was also below 2 m/s during the explosive growth stage. The modeled wind speed was to an extent higher than observed at the beginning and end in Xingtai. The trend of change in the modeled average wind speed for the Jing–Jin–Ji region showed reasonable agreement with observation and was closest to the observed situation in the explosive growth stage. In general, the modeled regional wind was higher than observed. Comparison of the wind speed among the three experiments showed that the wind speeds in EXP2 and EXP3 were basically same, but to a varying degree both were smaller than in EXP1 at Beijing and Xingtai, as well as for Jing–Jin–Ji as a whole, during the explosive growth stage, showing that AF decreased the surface wind speed. The trend of temperature change according to the three experiments was also consistent with observation, at Beijing, Xingtai, and Jing–Jin–Ji as a whole. However, it was found that the modeled temperature was obviously higher than observed, especially during the explosive growth stage. The temperature in EXP2 and EXP3 was basically same, but lower than in EXP1, which was much closer to observation, indicating that AF reduced the overestimation of surface temperature in Beijing, Xingtai, and

Jing–Jin–Ji as a whole. However, the temperature in EXP2 and EXP3 was also higher than observed during the explosive growth stage, suggesting a role played by other uncertainties in the PBL scheme besides AF, which is deserving of more detailed study in the future. Also shown in Figure 3 are the PBL-mean winds of the three experiments for Beijing, Xingtai, and Jing–Jin–Ji as a whole. Unfortunately, no observational data were available to evaluate them. However, comparison of the PBL's wind and temperature according to the three experiments showed that the PBL-mean wind was basically below 4 m/s while the temperature was high in the explosive stage at Beijing, Xingtai, and in Jing–Jin–Ji as a whole. Similar to the surface-level results, the PBL-mean wind speed and temperature in EXP2 and EXP3 were basically the same, but the wind speed in these two experiments was obviously lower than that in EXP1. This indicated that the reduction in wind speed by AF was more obvious in the PBL than at ground level. Meanwhile, comparison of the surface-level and PBL temperature of the three experiments showed that the cooling effect of AF was much stronger at the surface than in the PBL.

Aerosol optical properties, including AOD, SSA and asymmetry factor, largely determine the direct radiative effects of aerosols. The observed AOD (Table 4) and SSA (Table 5) at Shijiazhuang, Beijing and Xianghe were used to evaluate the modeled results for the period 15–22 December. Because the differences in the modeled AOD and SSA results of EXP1, EXP2 and EXP3 were small, those of EXP1 only are referred to here. The values of modeled AOD and SSA and their temporal trends of change during 15–22 December were basically consistent with observation at Beijing, Shijiazhuang and Xianghe, thus demonstrating good model performance in terms of its description of aerosol optical properties. Both the observed and modeled SSA at Shijiazhuang, Beijing and Xianghe (Table 5) showed that the SSA was obviously higher during the explosive growth stage compared with that at the beginning or end of the haze on 15–16 and 22 December, illustrating that the scattering characteristics of composite aerosols increase obviously when high AOD and $PM_{2.5}$ occur on severe haze days in the Jing–Jin–Ji region. The accurate description of AOD and SSA, especially with respect to the change in SSA from clean to haze days, is the basis of the following discussion on the effects of aerosols on $PM_{2.5}$.

Figure 4 displays the averaged observed $PM_{2.5}$ ($PM_{2.5}$_OBS) and simulated $PM_{2.5}$ of EXP1 ($PM_{2.5}$_EXP1), EXP2 ($PM_{2.5}$_EXP2) and EXP3 ($PM_{2.5}$_EXP3) during the explosive growth stage. It can be

seen from $PM_{2.5}$_OBS results that the averaged $PM_{2.5}$ values generally exceeded 100 μg/m^3 in east China, and Jing–Jin–Ji comprised the most polluted areas with $PM_{2.5}$ reaching 300–400 μg/m^3 in parts of Beijing, Tianjin, central-south Hebei, western Shandong, and northern Henan. The most polluted area with $PM_{2.5}$ values of 500–700 μg/m^3 appeared in southern Hebei and northern Henan provinces and the maximum value of $PM_{2.5}$ even exceeded 700 μg/m^3 in part area in southern Hebei. Comparison of $PM_{2.5}$_EXP1 and $PM_{2.5}$_OBS shows that $PM_{2.5}$_EXP1 was obviously lower than $PM_{2.5}$_OBS on the whole. Notably, EXP1 failed to simulate the $PM_{2.5}$ > 300 μg/m^3. $PM_{2.5}$_OBS was approximately 200–300 μg/m^3 over most of Shandong, while $PM_{2.5}$_bk was only 100–200 μg/m^3 in this region. Compared with $PM_{2.5}$_EXP1, the $PM_{2.5}$_EXP2 values were significantly improved by AF, and were much closer to $PM_{2.5}$_OBS. The high $PM_{2.5}$_OBS centers of 300–400, 400–500 and 500–600 μg/m^3 were almost simulated by EXP2, indicating the important effects of AF in simulating such high values of $PM_{2.5}$. However, the simulated areas of these centers were smaller than those of $PM_{2.5}$_OBS. EXP2 also failed to simulate the maximum $PM_{2.5}$ values over 600 μg/m^3 observed in southern Hebei. $PM_{2.5}$_EXP3 just about made up for this shortcoming; compared with $PM_{2.5}$_EXP1 and $PM_{2.5}$_EXP2, $PM_{2.5}$_EXP3 was undoubtedly the closest to $PM_{2.5}$_OBS both in terms of $PM_{2.5}$ extremes and the area of influence. These findings illustrate that both AF and decrease in turbulent diffusion coefficient in atmospheric chemistry models are required for the effective prediction of $PM_{2.5}$ explosive growth during severe haze in China's Jing–Jin–Ji region.

3.3 Change in downward solar radiation flux by aerosols and decrease in turbulent diffusion coefficient

PM in the atmosphere will inevitably lead to changes in surface and atmospheric solar radiation flux. When severe haze occurs, most PM is concentrated in the atmosphere near the surface and within the PBL; solar radiative flux reaching the ground is reduced greatly, which is a direct trigger for the subsequent changes in thermodynamics, dynamics, and then atmospheric stratification. Any factor leading to a change in the atmospheric PM loading might result in a change in the surface downward solar radiation flux (SDSRF). We calculated the percentage changes in SDSRF (W/m^2) between EXP2 and EXP1 [($SDSRF_{\_EXP2} - SDSRF_{\_EXP1}$) / $SDSRF_{\_EXP1}$], and EXP3 and EXP1 [($SDSRF_{\_EXP2} - SDSRF_{\_EXP1}$) / $SDSRF_{\_EXP1}$)], to study the impacts on SDSRF of aerosols and decrease in turbulent diffusion coefficient.

Figure 5 shows the mean percentage change in SDSRF (W/m^2) owing to aerosols (a) and aerosols plus decrease in turbulent diffusion coefficient, during the explosive growth stage. It can be seen that SDSRF was reduced by more than 50% by aerosols over most of the study region (60%–65% in Jing, Jin, most of Ji, and northern Shandong, and even 65%–70% in Jing, Jin, and part of Ji), indicating the important influence of aerosols on SDSRF. Comparison of Figures 5b and 5a shows that this reduction in SDSRF owing to aerosols (Figure 5a) in EXP2 was further strengthened by the decrease in turbulent diffusion coefficient of chemical tracers in EXP3 (Figure 5b) in certain regions, because decrease in turbulent diffusion coefficient led to the accumulation of more $PM_{2.5}$ near the surface (Figure 3), less transport and, subsequently, an increase in total $PM_{2.5}$ loading. It can also be seen that the difference between Figures 5a and 5b is negligible. This is because the major impact of decrease in turbulent diffusion coefficient was to reform the vertical distribution of the atmospheric loading of $PM_{2.5}$, and its impact on the total-column $PM_{2.5}$ was minor. On the other hand, the reduction in SDSRF owing to aerosol radiation was already considerable, and so the change in SDSRF owing to the increased total-column $PM_{2.5}$ by decrease in turbulent diffusion coefficient would be secondary. This value of SDSRF reduction owing to aerosols and decrease in turbulent diffusion coefficient is basically consistent with the 56%–89% difference of observational radiative exposure between clear and haze days during the same period (Zhong et al., 2018).

3.4 Influence of aerosols on the reforming of the local atmospheric temperature profile

Offline and online studies indicate a reforming of the atmospheric temperature profile owing to the direct effect of aerosol radiation (Wang et al., 2010, 2015b; Forkel et al., 2012; Gao et al., 2014, 2015; Wang et al., 2014; Gao et al., 2017; Ding et al., 2016). In our previous work (Wang et al., 2015a, 2015b), composite aerosol mixing of BC, OC, SF, NI, dust, ammonium, and sea salt aerosols was online coupled into the GRAPES_CAUCE model. On this basis, in the present study, the changes in the mean temperature profile of Jing–Jin–Ji during daytime owing to aerosol radiation were calculated for 15–20 December 2016. It can be seen from Figure 6 that aerosols cooled the atmosphere below 750–800 hPa, but warmed it above this height. Considering the PBL height may be as low as several hundreds to one thousand meters when severe haze occurs in Jing–Jin–Ji (Wang et al., 2015a; Zhong et al., 2017), it may be concluded that the whole PBL and its near upper atmosphere were cooled by aerosols to a varying extent during the different

315 stages of this haze process. The warming effects of aerosols above 750–850 hPa were very weak, and the
316 temperature differences among different days were also small. However, the cooling effects of aerosols
317 varied the most between different days from the surface to 975 hPa. For instance, surface daytime cooling
318 was about 2.2 K on 19 December, 1.5 K on 18 and 20 December, 1 K on 17 December, and 0.5–0.6 K on
319 15–16 December. This cooling effect of aerosols decreased rapidly with height. The difference in the
320 cooling rate between the surface and 850 hPa was 1.8 K on 19 December, 1.3 K on 18 and 20 December, 1
321 K on 17 December, and 0.3–0.4 K on 15 and 16 December. The difference in the cooling rate owing to
322 aerosols between the surface and the upper PBL was much bigger during the explosive growth stage than
323 the climbing stage. This may have resulted in further intensification of the temperature inversion layer that
324 already existed during the haze event, which will be discussed in the following section.

325 The meteorological data from the vertical soundings taken at Beijing and Xingtai were used to verify
326 this change in the temperature profile owing to aerosols. Figure 7 shows the vertical temperature profiles of
327 the sounding observations and the modeled temperature profiles of EXP1 and EXP2 during the climbing
328 stage (Figure 7a) and explosive growth stage (Figure 7b) at the two stations. The temperature profiles
329 (Figure 7a) show that the model results of EXP1 and EXP2 both simulated in part the observed temperature
330 inversion at Beijing and Xingtai on 15–16 December. The negligible difference between the temperature
331 profiles of EXP1 and EXP2 indicates that aerosol radiation had very little impact on the temperature
332 profiles and local inversion during the climbing stage. Nevertheless, Figure 7b shows that the observed
333 temperature inversions were obviously stronger and thicker on 18–19 December (explosive growth stage)
334 than those on 15–16 (climbing stage), both in Xingtai and Beijing. The temperate profiles of EXP2 were
335 much closer to the observational results than those of EXP1; and especially, the temperature inversions
336 were much stronger and also closer to observation than those of EXP1. This result proves that the
337 correction of local inversions by aerosols during the $PM_{2.5}$ explosive growth stage was effective.

338 However, it can also be seen that the inversions of EXP2, which included online AF, were still
339 weaker than observed at the two stations. This suggests there must be other reasons, besides the online
340 calculation of AF, for the underestimation of the observed extremely strong inversion by the model, which
341 is worthy of further study.

342 **3.5 Contributions of AF and decrease in turbulent diffusion coefficient to $PM_{2.5}$ explosive growth**

343 Turbulent diffusion is the main process of gas and particle exchange from surface to upper atmosphere,
344 and removal by high-altitude transport, and one of the key tasks of atmospheric chemistry models is to
345 capture this process. Firstly, the inversion and weak turbulent diffusion, which generates from atmospheric
346 dynamic processes, leads to atmospheric stabilization and determines the occurrence of haze and its
347 strength (Zheng et al., 2016). Once the haze occurs, aerosol radiation may in turn reinforce the inversion
348 when aerosols exceed a certain critical value, leading to more $PM_{2.5}$ gathering near the ground. The relative
349 importance of these two aspects on $PM_{2.5}$ explosive growth may vary with $PM_{2.5}$ concentrations and
350 meteorological conditions, but they are irreplaceable for a reasonable prediction and simulation of $PM_{2.5}$
351 explosive growth and peaks in atmospheric models.

352 Figure 8 displays the hourly change in observed $PM_{2.5}$ ($PM_{2.5}$_OBS) and the modeled $PM_{2.5}$ of EXP1,
353 EXP2 and EXP3, together with the modeled turbulent diffusion coefficient of the three experiments, in
354 Beijing (Figure 8a) and Xingtai (Figure 8b), for the period 15–23 December. Comparison of the $PM_{2.5}$
355 modeled by EXP1, EXP2 and EXP3 with observation in Beijing (Figure 8a) shows that the $PM_{2.5}$ modeled
356 by EXP3 was the closest to observation during the whole haze episode, which agreed with the results of the
357 regional distribution of the explosive growth stage illustrated in Figure 4. EXP1 underestimated the $PM_{2.5}$
358 obviously during 17–22 December, and this underestimation was even more obvious with increasing $PM_{2.5}$.
359 This difference between the modeled and observed $PM_{2.5}$ was largest during the explosive growth stage. AF
360 reduced this difference to a considerable extent, and the $PM_{2.5}$ of EXP2 was much closer to observation
361 than that of EXP1 during the explosive growth stage. However, there were certain differences between the
362 observed and $PM_{2.5}$ and that modeled by EXP2, illustrating that AF cannot completely fill the sizeable gap
363 between observed and modeled $PM_{2.5}$. The $PM_{2.5}$ of EXP3 reduced this gap further, showing the best
364 agreement with observation, especially during the $PM_{2.5}$ explosive growth stage.

365 It can also be seen from Figure 8a that the diffusion coefficient of EXP1 was about 30–40 m^2/s during
366 the explosive growth stage, which was about 50% of the 60–70 m^2/s on clear days (15 or 22 December).
367 Obviously, this 50% diffusion coefficient difference between clear and severe haze days may be insufficient
368 to separate the difference in turbulent diffusion intensity between the extremely stable atmosphere on haze

days and the unstable atmosphere on clear days, which is an important reason for the underestimated $PM_{2.5}$ explosive growth in EXP1. Compared with EXP1, the AF in EXP2 led to a notable enhancement of the temperature inversion (Figure 7b), a significant decrease in the turbulent diffusion of $PM_{2.5}$ during the explosive growth stage, and a low maximum diffusion coefficient at noon (as low as 14 m^2/s on 20 December – a reduction of 50% compared with EXP1). The maximum diffusion coefficient at noon on haze days in EXP2 was only about 20% of that on clear days. The maximum diffusion coefficient at noon in EXP3 was lower than 5 m^2/s on 20 December and, at the same time, the $PM_{2.5}$ modeled by EXP3 was further increased and was also much closer to the observed $PM_{2.5}$ than the $PM_{2.5}$ of EXP2.

Through comparison of the temporal change of diffusion coefficient and $PM_{2.5}$ in EXP1, EXP2 and EXP3 in Beijing, it is clear that an overestimation of turbulent diffusion coefficient owing to the absence of online-calculated AF, as well as a deficient description of extremely stable stratification in the PBL scheme of the atmospheric model, can lead to a distinct underestimation of $PM_{2.5}$ explosive growth and peaks when severe haze occurs in China's Jing–Jin–Ji region.

The trends of change in diffusion coefficient and $PM_{2.5}$ at Xingtai in the three experiments (Figure 8b) are similar to those at Beijing. The $PM_{2.5}$ of EXP3 was also closest to observation, followed by EXP2, and then EXP1 was the worst, during the whole haze episode. However, during the explosive growth stage, the relative contributions of AF and decrease in turbulent diffusion coefficient to the $PM_{2.5}$ peak values showed some differences to those at Beijing. The contributions of decrease in turbulent diffusion coefficient to $PM_{2.5}$ peaks were more important than those of AF at Xingtai. Located in the eastern foothills of the Taihang Mountains, Xingtai is usually affected by downhill airflow. Temperature inversions in this area form and strengthen easily, leading to stronger inversion, weaker turbulent diffusion, and more stable atmospheric stratification. However, this kind of inversion and weak turbulent diffusion, derived from the local terrain, is harder for PBL schemes in atmospheric chemistry models to describe, and likely underestimated.

Figure 9 is a diagrammatic sketch of the contributions of AF and decrease in turbulent diffusion coefficient to the $PM_{2.5}$ of the explosive growth stage according to the results at Beijing and Xingtai. It can be seen that the diffusion coefficient of EXP1 was 30–35 m^2/s, while that of EXP2 was 15–17 m^2/s,

meaning AF reduced the diffusion coefficient by about 43%–57%, which led to the rise in simulated $PM_{2.5}$ from 144 ug/m^3 in EXP1 to 205 ug/m^3 in EXP2 at Beijing, and from 280 ug/m^3 in EXP1 to 360 ug/m^3 in EXP2 at Xingtai. This means that AF reduced the underestimation of $PM_{2.5}$ at Beijing and Xingtai by 20% and 25%, respectively. The diffusion coefficient of EXP3 was as low as 4–6 m^2/s during the explosive growth stage, demonstrating the joint effects of AF and decrease in turbulent diffusion coefficient reduced the diffusion coefficient to less than 4–6 m^2/s, near-zero, which we refer to as "turbulent intermittence". The direct result of this "turbulent intermittence" was a further increase in the simulated surface $PM_{2.5}$, Based on EXP2, the further decrease in turbulent diffusion coefficient reduced the underestimation of simulated $PM_{2.5}$ by 14% to 20%, and the $PM_{2.5}$ errors in EXP3 were reduced to as low as −11% to 2%.

4. Conclusions

Using an atmospheric chemistry model, GRAPES_CUACE, three experiments (EXP1, EXP2 and EXP3) were designed to study the reason for the explosive growth of $PM_{2.5}$ mass during a "red-alert" heavy haze event that occurred during 15–23 December 2016 in China's Jing–Jin–Ji region. The contributions of AF and decrease in turbulent diffusion coefficient to the $PM_{2.5}$, representing compensation for the deficient description of extremely weak turbulent diffusion in the PBL scheme of the atmospheric model, were studied by analyzing the changes in $PM_{2.5}$, SDSRF, wind speed and temperature, diffusion coefficient, and the relationships among them, in the three experiments.

Results show that the diffusion coefficient in EXP1 was about 60–70 m^2/s on clear days and 30–35 m^2/s on haze days. The 50% difference between the two was considered insufficient to separate the unstable atmosphere on clear days and the extreme stable atmosphere on severe haze days, compared with the differences in direct downward solar radiation between clear and haze days, which was also proven indirectly by the weaker inversion of EXP1 than that from sounding observations. This led to a 40%–51% underestimation of the $PM_{2.5}$ peaks in EXP1 during the $PM_{2.5}$ explosive growth stage. Online calculation of AF reduced the surface and PBL wind speed and cooled the surface and PBL atmosphere. The surface daytime cooling due to aerosol radiation was 1.5–2.2 K during the explosive growth stage and 0.5–0.6 K during the climbing stage. The cooling effect of aerosols decreased rapidly with height, and this was a major reason for the strengthening of the temperature inversion during the explosive growth stage. The

423 reduced diffusion coefficient owing to AF reached 43%–57% during the $PM_{2.5}$ explosive growth stage. The
424 local inversion simulated in EXP2 was strengthened and closer to the actual sounding observation than that
425 of EXP1. This resulted in a 20%–25% reduction in the underestimation of $PM_{2.5}$, with $PM_{2.5}$ errors in EXP2
426 being as low as −16 to −11% during the explosive growth stage. The impact on $PM_{2.5}$ owing to AF in the
427 model run was distinct during the explosive growth stage, but minor during the climbing stage, indicating a
428 critical value of 150 ug/m^3 of $PM_{2.5}$ leading to an effective AF in online atmospheric chemistry models.
429 However, the local inversion simulated by EXP2 was still weaker than observed, and the $PM_{2.5}$ of EXP2
430 was still smaller than observed, illustrating AF could not solve all the $PM_{2.5}$ underestimation problems. In
431 EXP3, the decrease in turbulent diffusion coefficient of particles and gas based on EXP2 resulted in a
432 14%–20% lessening of the $PM_{2.5}$ underestimation based on EXP2, and the $PM_{2.5}$ errors of EXP3 were
433 reduced to −11% to 2%.

434 The present study illustrates that the PBL schemes in current atmospheric chemistry models are
435 probably insufficient for describing the extremely stable atmosphere resulting in explosive growth of $PM_{2.5}$
436 and severe haze in China's Jing–Jin–Ji region. This may involve two important reasons: the absence of an
437 online calculation of AF, and/or a deficient description of extremely weak turbulent diffusion by the PBL
438 scheme in the atmospheric chemistry model. Our study suggests that an online calculation of AF and an
439 improvement in the representation of turbulent diffusion in PBL schemes, with a focus on extremely stable
440 atmospheric stratification, in atmospheric chemistry models, are indispensable for a reasonable description
441 of local "turbulent intermittence" and an accurate prediction of the explosive growth and peaks of $PM_{2.5}$ of
442 severe haze in China's Jing–Jin–Ji region.
443
444

Author Contributions:

Hong Wang and Xiaoye Zhang designed the idea and experiments; Hong Wang and Yue Peng carried them out; Hongli Liu prepared the emissions data and introduction; Meng Zhang performed some of the model runs; Huizheng Che and Yu Zheng processed the AOD and SSA observational data; Yanli Cheng completed Table 3 and the related introduction.

Acknowledgements

This study was supported by the National Key Project (2016YFC0203306), the National Natural Science Foundation of China (41590874), and the National (Key) Basic Research and Development (973) Program of China (2014CB441201).

References

Basu, S., Iyengar, G. R., and Mitra, A. K.: Impact of a nonlocal closure scheme in a simulation of a monsoon system over India. Mon. Wea. Rev., 130, 161–170, 2002.

Bright, D. R., and Mullen, S. L.: The sensitivity of the numerical simulation of the southwest monsoon boundary layer to the choice of PBL turbulence parameterization in MM5, Wea. Forecasting, 17, 99–114, 2002.

Caplan, P., Derber, J., Gemmill, W., Hong, S.-Y., Pan, H.-L., and Parrish, D.: Changes to the 1995 NCEP operational medium-range forecast model analysis-forecast system, Wea. Forecasting, 12, 581–594, 1997.

Che, H., Zhang, X., Chen, H., Damiri, B., Goloub, P., Li, Z., Zhang, X., Wei, Y., Zhou, H., Dong, F., Li, D., and Zhou, T.: Instrument calibration and aerosol optical depth validation of the China Aerosol Remote Sensing Network, J. Geophys. Res. Atmos., 114, D03206, doi:10.1029/2008JD011030, 2009.

Che, H., Xia, X., Zhu, J., Li, Z., Dubovik, O., Holben, B., Goloub, P., Chen, H., Estelles, V., Cuevas-Agulló, E., Blarel, L., Wang, H., Zhao, H., Zhang, X., Wang, Y., Sun, J., Tao, R., Zhang, X., and Shi, G.: Column aerosol optical properties and aerosol radiative forcing during a serious haze-fog month over North China Plain in 2013 based on ground-based sunphotometer measurements, Atmos. Chem.Phys., 14, 2125–2138, doi:10.5194/acp-14-21252014, 2014.

Che, H., Zhang, X.-Y., Xia, X., Goloub, P., Holben, B., Zhao, H., Wang, Y., Zhang, X. C., Wang, H., Blarel,

L., Damiri, B., Zhang, R., Deng, X., Ma, Y., Wang, T., Geng, F., Qi, B., Zhu, J., Yu, J., Chen, Q., and Shi, G.: Ground-based aerosol climatology of China: aerosol optical depths from the China Aerosol Remote Sensing Network (CARSNET) 2002–2013, Atmos. Chem. Phys., 15, 7619–7652, https://doi.org/10.5194/acp15-7619-2015, 2015.

Chen, D., Xue, J., Yang, X., Zhang, H., Shen, X., Hu, J., Wang, Y., Ji, L., and Chen, J.: New generation of multi-scale NWP system (GRAPES): general scientific design, Chinese Sci. Bull., 53, 3433–3445, doi:10.1007/s11434-008-0494-z, 2008.

Chou, M. D., Suarez, M. J., Ho, C. H., Yan, M. M. H., and Lee, K. T.: Parameterizations for Cloud Overlapping and Shortwave Single-Scattering Properties for Use in General Circulation and Cloud Ensemble Models, J. Clim., 11, 202–214, 1998.

Chou, M. D., Suarez, M. J., Liang, X. Z., and Michael M.-H. Y.: A Thermal Infrared Radiation Parameterization for Atmospheric Studies, Technical Report Series on Global Modeling and Data Assimilation, NASA/TM-2001-104606, 19, America, Goddard Space Flight Center, Greenbelt, Maryland, 55, 2001.

Ding, A. J., Fu, C. B., Yang, X. Q., Sun, J. N., Petäjä, T., Kerminen, V. M., Wang, T., Xie, Y., Herrmann, E., Zheng, L. F., Nie, W., Liu, Q., Wei, X. L., and Kulmala, M.: Intense atmospheric pollution modifies weather: a case of mixed biomass burning with fossil fuel combustion pollution in eastern China, Atmos. Chem. Phys., 13, 10545-10554, 2013.

Ding, A. J., Huang, X., Nie, W., Sun, J. N., Kerminen, V. M., Petäjä, T., Su, H., Cheng, Y. F., Yang, X. Q., Wang, M. H., Chi, X. G., Wang, J. P., Virkkula, A., Guo, W. D., Yuan, J., Wang, S. Y., Zhang, R. J., Wu, Y. F., Song, Y., Zhu, T., Zilitinkevich, S., Kulmala, M., and Fu, C. B.: Enhanced haze pollution by black carbon in megacities in China, Geophys. Res. Lett., 43, 2873-2879, 2016.

Farfán, L. M., and Zehnder, J. A.: An analysis of the landfall of Hurricane Nora (1997), Mon. Wea. Rev., 129, 2073–2088, 2001.

Forkel, R., Werhahn, J., Hansen, A. B., McKeen, S., Peckham, S., Grell, G., and Suppan, P.: Effect of aerosol-radiation feedback on regional air quality – A case study with WRF/Chem, Atmos. Environ., 53, 202-211, 2012.

499 Fountoukis, C., and Nenes A., ISORROPIA II: a computationally efficient thermodynamic equilibrium
500 model for K+–Ca2+–Mg2+–NH+4 –Na+–SO2−4 –NO−3 –Cl−–H2O aerosols, Atmos. Chem. Phys.,
501 2007, 7, 4639–4659.
502 Gal-Chen, T., and Sommerville, R. C. J.: On the use of a coordinate transformation for the solution of the
503 Navier-Stokes equations, J. Comput. Phys., 17, 209—228, 1975.
504 Gao, Y., Zhao, C., Liu, X., Zhang, M., and Leung, L. R.: WRF-Chem simulations of aerosols and
505 anthropogenic aerosol radiative forcing in East Asia, Atmos. Environ., 92, 250-266, 2014.
506 Gao, Y., Zhang, M., Liu, Z., Wang, L., Wang, P., Xia, X., Tao, M., and Zhu, L.: Modeling the feedback
507 between aerosol and meteorological variables in the atmospheric boundary layer during a severe fog–
508 haze event over the North China Plain, Atmos. Chem. Phys., 15, 4279-4295, 2015.
509 Gao, M., Carmichael, G. R., Saide, P. E., Lu, Z., Yu, M., Streets, D. G., and Wang, Z.: Response of winter
510 fine particulate matter concentrations to emission and meteorology changes in North China, Atmos.
511 Chem. Phys., 16, 11837-11851, 2016.
512 Gao, M., Saide, P. E., Xin, J., Wang, Y., Liu, Z., Wang, Y., Wang, Z., Pagowski, M., Guttikunda, S.K., and
513 Carmichael, G. R.: Estimates of Health Impacts and Radiative Forcing in Winter Haze in Eastern
514 China through Constraints of Surface PM2.5 Predictions, Environ. Sci. Technol., 51, 2178-2185, 2017.
515 Gong, S., and Zhang, X.: CUACE/Dust-an integrated system for operational dust forecasting in Asia,
516 Computers & Applied Chemistry, 25, 1061-1067, 2008.
517 Gong, S. L., Lavoué, D., Zhao, T. L., Huang, P., and Kaminski, J. W.: GEM-AQ/EC, an on-line global
518 multi-scale chemical weather modelling system: model development and evaluation of global aerosol
519 climatology, Atmos. Chem. Phys., 12, 8237–8256, doi:10.5194/acp-12-8237-2012, 2012.
520 Grell, G. A., Dudhia, J., and Stauffer, D.: A description of the fifth-generation PENN State/NCAR
521 Mesoscale Model (MM5). NCAR Tech. Note NCAR/TN-398 STR, 138, 1994.
522 He, K.: Multi-resolution Emission Inventory for China (MEIC): model framework and 1990-2010
523 anthropogenic emissions, AGU Fall Meeting, AGU Fall Meeting Abstracts, 2012.
524 Holben B. N., Eck, T .F., Slutsker, I,, et al. AERONET—A Federated Instrument Network and Data
525 Archive for Aerosol Characterization, 1998.

526 Hong, S. Y. and Pan, H. L.: Nonlocal boundary layer vertical diffusion in a Medium-Range Forecast model,
527 Mon. Weather Rev., 124, 2322–2339, 1996.
528 Hong, S. Y., Noh, Y., and Dudhia, J.: A New Vertical Diffusion Package with an Explicit Treatment of
529 Entrainment Processes, Mon. Weather Rev., 134, 2318-2341, 2006.
530 Hu, X. M., Doughty, D. C., Sanchez, K. J., Joseph, E., and Fuentes, J. D.: Ozone variability in the
531 atmospheric boundary layer in Maryland and its implications for vertical transport model, Atmos.
532 Environ., 46, 354-364, 2012.
533 Hu, X. M., Klein, P. M., and Xue, M.: Evaluation of the updated YSU planetary boundary layer scheme
534 within WRF for wind resource and air quality assessments, J. Geophys. Res. Atmos., 118,
535 10490-10505, 2013a.
536 Hu, X. M., Klein, P. M., Xue, M., Zhang, F., Doughty, D. C., Forkel, R., Joseph, E., and Fuentes, J. D.:
537 Impact of the vertical mixing induced by low-level jets on boundary layer ozone concentration, Atmos.
538 Environ., 70, 123-130, 2013b.
539 Hua, Y., Wang, S., Wang, J., Jiang, J., Zhang, T., Song, Y., Kang, L., Zhou, W., Cai, R., Wu, D., Fan, S.,
540 Wang, T., Tang, X., Wei, Q., Sun, F., and Xiao, Z.: Investigating the impact of regional transport on
541 PM2.5 formation using vertical observation during APEC 2014 Summit in Beijing, Atmos. Chem.
542 Phys., 16, 15451–15460, 2016.
543 Huang, R. J., Zhang, Y., Bozzetti, C., Ho, K. F., Cao, J. J., Han, Y., Daellenbach, K. R., Slowik, J. G., Platt,
544 S. M., Canonaco, F., Zotter, P., Wolf, R., Pieber, S. M., Bruns, E. A., Crippa, M., Ciarelli, G.,
545 Piazzalunga, A., Schwikowski, M., Abbaszade, G., Schnelle-Kreis, J., Zimmermann, R., An, Z., Szidat,
546 S., Baltensperger, U., El Haddad, I., and Prevot, A. S.: High secondary aerosol contribution to
547 particulate pollution during haze events in China, Nature, 514, 218-222, 2014.
548 Jiang, C., Wang, H., Zhao, T., Li, T., and Che, H.: Modeling study of PM2.5 pollutant transport across cities
549 in China's Jing–Jin–Ji region during a severe haze episode in December 2013, Atmos. Chem. Phys., 15,
550 5803-5814, 2015.
551 Kain, J. S. and Fritsch, J. M.: Convection parameterization for mesoscale models: the Kain-Fritsch scheme,
552 Meteor. Mon., 24, 165–170, 1993.

553 Kusaka, H., Kondo, H., Kikegawa, Y., and Kimura, F.: A simple single-layer urban canopy model for
554 atmospheric models: Comparison with multi-layer and slab models. Bound.-Layer Meteor., 101, 329–
555 358, 2001.
556 Li, K., Liao, H., Zhu, J., and Moch, J. M.: Implications of RCP emissions on future PM2.5 air quality and
557 direct radiative forcing over China, J. Geophys. Res. Atmos., 121, 12985-13008, 2016.
558 Li, T., Wang, H., Zhao, T., Xue, M., Wang, Y., Che, H., and Jiang, C.: The Impacts of Different PBL
559 Schemes on the Simulation of PM2.5 during Severe Haze Episodes in the Jing-Jin-Ji Region and Its
560 Surroundings in China, Adv. Meteorol., 1-15, 2016.
561 Lim, K. S. S., and Hong, S. Y.: Development of an effective double-moment cloud microphysics scheme
562 with prognostic cloud condensation nuclei (CCN) for weather and climate models, Mon. Wea. Rev.,
563 138, 1587-1612, 2010.
564 Mass, C. F., D. Ovens, K. Westrick, and B. A. Colle: Does increasing horizontal resolution proxduce more
565 skilful forecasts? Bull. Amer. Meteor. Soc., 83, 407–430, 2002.
566 Miao, Y., Liu, S., Zheng, Y., and Wang, S.: Modeling the feedback between aerosol and boundary layer
567 processes: a case study in Beijing, China, Environ. Sci. Pollut R., 23, 3342-3357, 2016.
568 Petäjä, T., Järvi, L., Kerminen, V. M., Ding, A. J., Sun, J. N., Nie, W., Kujansuu, J., Virkkula, A., Yang, X.
569 Q., Fu, C. B., Zilitinkevich, S., and Kulmala, M.: Enhanced air pollution via aerosol-boundary layer
570 feedback in China, Sci. Rep., 6, 18998, 2016.
571 Pleim, J.: A combined local and non-local closure model for the atmospheric boundary layer. Part II:
572 Application and evaluation in a mesoscale meteorological model, J. Applied Meteor. Climatology, 46,
573 1396–1409, 2007.
574 Qiu, Y., Liao, H., Zhang, R., and Hu, J.: Simulated impacts of direct radiative effects of scattering and
575 absorbing aerosols on surface layer aerosol concentrations in China during a heavily polluted event in
576 February 2014, J. Geophys. Res. Atmos., 122, 5955-5975, 2017.
577 Quan, J., Tie, X., Zhang, Q., Liu, Q., Li, X., Gao, Y., and Zhao, D.: Characteristics of heavy aerosol
578 pollution during the 2012–2013 winter in Beijing, China, Atmos. Environ., 88, 83-89, 2014.
579 Stockwell, W. R., Middleton, P., Chang, J. S., and Tang, X.: The Second Generation Regional Acid

580 Deposition Model Chemical Mechanism for Regional Air Quality Modeling, J. Geophys. Res., 95,
581 16343-16376, 1990.
582 Sun, Y., Jiang, Q., Wang, Z., Fu, P., Li, J., Yang, T., and Yin, Y.: Investigation of the sources and evolution
583 processes of severe haze pollution in Beijing in January 2013, J. Geophys. Res. Atmos., 119,
584 4380-4398, 2014.
585 Wang, H., Gong, S., Zhang, H., Chen, Y., Shen, X., Chen, D., Xue, J., Shen, Y., Wu, X., and Jin, Z.: A
586 new-generation sand and dust storm forecasting system GRAPES_CUACE/Dust: Model development,
587 verification and numerical simulation, Chinese Sci. Bull., 55, 635-649, 2009.
588 Wang, H., Zhang, X., Gong, S., Chen, Y., Shi, G., and Li, W.: Radiative feedback of dust aerosols on the
589 East Asian dust storms, J. Geophys. Res., 115 , D23214, 2010.
590 Wang, H., Tan, S. C., Wang, Y., Jiang, C., Shi, G. Y., Zhang, M. X., and Che, H. Z.: A multi sources
591 observation study of the severe prolonged regional haze episode over eastern China in January 2013,
592 Atmos. Environ., 89, 807-815, 2014a.
593 Wang, H., Xu, J., Zhang, M., Yang, Y., Shen, X., Wang, Y., Chen, D., and Guo, J.: A study of the
594 meteorological causes of a prolonged and severe haze episode in January 2013 over central-eastern
595 China, Atmos. Environ., 98, 146-157, 2014b.
596 Wang, H., Xue, M., Zhang, X. Y., Liu, H. L., Zhou, C. H., Tan, S. C., Che, H. Z., Chen, B., and Li, T.:
597 Mesoscale modeling study of the interactions between aerosols and PBL meteorology during a haze
598 episode in Jing–Jin–Ji (China) and its nearby surrounding region – Part 1: Aerosol distributions and
599 meteorological features, Atmos. Chem. Phys., 15, 3257-3275, 2015a.
600 Wang, H., Shi, G. Y., Zhang, X. Y., Gong, S. L., Tan, S. C., Chen, B., Che, H. Z., and Li, T.: Mesoscale
601 modelling study of the interactions between aerosols and PBL meteorology during a haze episode in
602 China Jing–Jin–Ji and its near surrounding region - Part 2: Aerosols' radiative feedback effects, Atmos.
603 Chem. Phys., 15, 3277-3287, 2015b.
604 Wang, J., Wang, S., Jiang, J., Ding, A., Zheng, M., Zhao, B., Wong, D. C., Zhou, W., Zheng, G., Wang, L.,
605 Pleim, J. E., and Hao, J.: Impact of aerosol–meteorology interactions on fine particle pollution during
606 China's severe haze episode in January 2013, Environ. Res. Lett., 9, 094002, 2014.

607 Wang, Y., Zhang, Q. Q., He, K., Zhang, Q., and Chai, L.: Sulfate-nitrate-ammonium aerosols over China:
608 response to 2000–2015 emission changes of sulfur dioxide, nitrogen oxides, and ammonia, Atmos.
609 Chem. Phys., 13, 2635-2652, 2013.
610 Wang, Z., Li, J., Wang, Z., Yang, W., Tang, X., Ge, B., Yan, P., Zhu, L., Chen, X., Chen, H., Wand, W., Li,
611 J., Liu, B., Wang, X., Wand, W., Zhao, Y., Lu, N., and Su, D.: Modeling study of regional severe hazes
612 over mid-eastern China in January 2013 and its implications on pollution prevention and control, Sci.
613 China Earth Sci., 57, 3-13, 2014.
614 Xu, G., Chen, D., Xue, J., Sun, J., Shen, X., Shen, Y., Huang, L., Wu, X., Zhang, H., and Wang, S.: The
615 program structure designing and optimizing tests of GRAPES physics, Chinese Sci. Bull., 53, 3470–
616 3476, doi:10.1007/s11434-008-0418-y, 2008.
617 Yang, Y., Liao, H., and Lou, S.: Increase in winter haze over eastern China in recent decades: Roles of
618 variations in meteorological parameters and anthropogenic emissions, J. Geophys. Res. Atmos., 121,
619 13050-13065, 2016.
620 Yang, X., Hu, J., Chen, D., Zhang, H., Shen, X., Chen, J., and Ji, L.: Verification of GRAPES unified global
621 and regional numerical weather prediction model dynamic core, Chinese Sci. Bull., 53, 3458–3464,
622 doi:10.1007/s11434-008-0417-z, 2008.
623 Yang, X. S., Chen, J. B., and Hu, J. L.: A semi-implicit semi-Lagran global nonhydrostatic model and the
624 polar discretization scheme, Sci. China Ser D-Earth Sci., 50,1885-1891, 2007.
625 Yang, Y. R., Liu, X. G., Qu, Y., An, J. L., Jiang, R., Zhang, Y. H., Sun, Y. L., Wu, Z. J., Zhang, F., Xu, W. Q.,
626 and Ma, Q. X.: Characteristics and formation mechanism of continuous hazes in China: a case study
627 during the autumn of 2014 in the North China Plain, Atmos. Chem. Phys., 15, 8165–8178,
628 doi:10.5194/acp-158165-2015, 2015.
629 Zhang, M., Wang, H., Zhang, X., Peng, Y., and Che, H.: Applying the WRF double-moment six-class
630 microphysics scheme in the GRAPES_Meso model: A case study, J. Meteor. Res., 32, 246, doi:
631 10.1007/s13351018-7066-1, 2018.
632 Zhang, R., and Shen, X.: On the development of the GRAPES – a new generation of the national
633 operational NWP system in China, Chinese Sci. Bull., 53, 3429–3432, doi:10.1007/s11434008-0462-7,

2008.

Zhang, R. H., Li, Q., and Zhang, R. N.: Meteorological conditions for the persistent severe fog and haze event over eastern China in January 2013, Sci. China Earth Sci., 57, 26–35, 2014.

Zheng, G. J., Duan, F. K., Su, H., Ma, Y. L., Cheng, Y., Zheng, B., Zhang, Q., Huang, T., Kimoto, T., Chang, D., Pöschl, U., Cheng, Y. F., and He, K. B.: Exploring the severe winter haze in Beijing: the impact of synoptic weather, regional transport and heterogeneous reactions, Atmos. Chem. Phys., 15, 2969–2983, doi:10.5194/acp-15-2969-2015, 2015.

Zheng,G.J.,Duan,F.K.,Ma,Y.L.,Zhang,Q.,Huang,T.,Kimoto, T. K., Cheng, Y. F., Su, H., and He, K. B.: Episode-based evolution pattern analysis of haze pollution: method development and results from Beijing, China, Environ. Sci. Technol., 50, 4632– 4641, 2016.

Zhong, J., Zhang, X., Dong, Y., Wang, Y., Liu, C., Wang, J., Zhang, Y., and Che, H.: Feedback effects of boundary-layer meteorological factors on cumulative explosive growth of PM2.5 during winter heavy pollution episodes in Beijing from 2013 to 2016, Atmos. Chem. Phys., 18, 247–258, https://doi.org/10.5194/acp18-247-2018, 2018a.

Zhong, J., Zhang, X., Wang, Y., Liu, C., and Dong, Y.: Heavy aerosol pollution episodes in winter Beijing enhanced by radiative cooling effects of aerosols, Atmos. Res., 209, 59-64, 2018b.

Zhong, J., Zhang, X., Wang, Y., Sun, J., Zhang, Y., Wang, J., Tan, K., Shen, X., Che, H., and Zhang, L.: Relative contributions of boundary-layermeteorologicalfactorstotheexplosivegrowthof PM 2.5 during the red-alert heavy pollution episodes in Beijing in December 2016, J Meteorol. Res., 31, 809–819, 2017.

Zhou, C., Gong, S., Zhang, X., Liu, H., Xue, M., Cao, G., An, X., Che, H., Zhang, Y., and Niu, T.: Towards the improvements of simulating the chemical and optical properties of Chinese aerosols using an online coupled model CUACE/Aero, Tellus B, 64, 18965, doi:10.3402/tellusb.v64i0.18965, 2012.

Zhou, C., Zhang, X., Gong, S., Wang, Y., and Xue, M.: Improving aerosol interaction with clouds and precipitation in a regional chemical weather modeling system, Atmos. Chem. Phys., 16, 145-160, 2016.

Table 1. Physical and chemical processes in GRAPES_CUACE

Process	Option	Reference
Explicit precipitation	WDM6	Lim and Hong (2010)
Cumulus cloud	KFETA scheme	Kain (2004)
Longwave radiation	Goddard	Chou et al. (2001)
Shortwave radiation	Goddard	Chou et al. (1998)
Surface layer	SFCLAY scheme	Pleim (2007)
PBL	MRF scheme	Hong et al. (1996, 2006)
Land surface	SLAB scheme	Kusaka et al. (2001)
Gas-phase chemistry	RADM II	Stockwell et al. (1990)
Aerosol	CUACE	Zhou et al. (2012)
Aerosol direct effect	External mixing	Wang et al. (2015)
Aerosol indirect effect	CAUCE+WDM6	Zhou et al. (2016)

679

680

681 Table 2. Design of sensitivity experiments

Experiment	Description
EXP1	Background experiment: ignoring aerosol radiation and conventional diffusion coefficient of chemical tracers by PBL scheme in GRAPES_CUACE
EXP2	Online AF online and conventional diffusion coefficient of chemical tracers by PBL scheme in GRAPES_CUACE
EXP3	Online AF and DC of chemical tracers set to 20% of conventional diffusion coefficient calculated by PBL scheme, representing compensation for the deficient description of extremely weak turbulent diffusion by the PBL scheme; diffusion coefficient in physical and dynamic processes the same as EXP1

682

683

Table 3. VOCs in the emissions data

VOC	Full name
ALD	Acetaldehyde and higher aldehydes
CH4	Methane
CSL	Cresol and other hydroxy substituted aromatics
ETH	Ethane
HC3	Alkanes w/ $2.7 \times 10^{-13} > kOH < 3.4 \times 10^{-12}$
HC5	Alkanes w/ $3.4 \times 10^{-12} > kOH < 6.8 \times 10^{-12}$
HC7	$w/kOH > 6.8 \times 10^{-12}$
HCHO	Formaldehyde
ISOP	Isoprene
KET	Ketones
OL2	Ethene
OLI	Internal olefins
OLT	Terminal olefins
ORA2	Acetic and higher acids
PAR	Paraffin carbon bond
TERPB	Monoterpenes
TOL	Toluene and less reactive aromatics
XYL	Xylene and more reactive aromatics

Table 4. Observed and modeled daily AOD (* stands for shortage of observation)

Date	Shijiazhuang		Beijing		Xianghe	
	OBS	MODEL	OBS	MODEL	OBS	MODEL
15	0.46	0.55	0.07	0.12	0.10	0.15
16	0.62	0.60	0.14	0.18	0.60	0.40
17	1.30	1.10	0.50	0.56	1.33	1.05
18	1.42	1.20	0.69	0.75	0.87	0.97
19	1.26	1.30	0.50	0.86	0.96	0.90
20	*	1.20	1.90	1.70	*	1.50
21	*	0.65	1.76	1.50	1.78	1.60
22	0.18	0.30	0.10	0.20	0.18	0.22

Table 5. Observed and modeled daily SSA (* stands for shortage of observation).

Date	Shijiazhuang		Beijing		Xianghe	
	OBS	MODEL	OBS	MODEL	OBS	MODEL
15	0.83	0.85	0.81	0.83	0.86	0.84
16	0.83	0.85	0.88	0.86	0.92	0.86
17	0.88	0.89	0.88	0.90	0.93	0.90
18	0.87	0.89	0.91	0.92	0.90	0.90
19	0.86	0.91	0.90	0.93	0.92	0.91
20	*	0.90	*	0.93	*	0.92
21	*	0.88	0.93	0.93	*	0.90
22	0.82	0.83	0.84	0.86	0.88	0.84

Figure captions

Fig. 1. (a) Model domain and location of Jing–Jin–Ji. (b) Geographic location and topography of Jing–Jin–Ji. Blue dots are the locations of $PM_{2.5}$ observations; red triangles are the locations of automatic weather stations; yellow stars are the two sounding stations; black crosses are the CARSNET and AEROSNET stations.

Fig. 2. Geopotential height (color-shaded; gp10m), temperature (dashed black contours; K) and wind (wind bars; m/s) in the (a) upper (500 hPa) and (b) middle (700 hPa) atmosphere, and geopotential height and wind in the (c) lower atmosphere (850 hPa) and (d–f) PBL (900, 950, 1000 hPa), at 0000 UTC 19 December 2016.

Fig. 3. Observed and modeled wind speed and temperature at the surface (upper panels), and the PBL-mean wind speed and temperature (lower panels), from the results of EXP1, EXP2 and EXP3 for Beijing, Xingtai, and the average for Jing–Jin–Ji as a whole, during 15–24 December 2016.

Fig. 4. Mean observed (OBS_$PM_{2.5}$) and modeled $PM_{2.5}$ concentration ($\mu g/m^3$) of the $PM_{2.5}$ explosive growth stage, from the results of EXP1, EXP2 and EXP3 ($PM_{2.5}$_EXP1, $PM_{2.5}$_EXP2 and $PM_{2.5}$_ EXP3, respectively).

Fig. 5. Mean percentage change in SDSRF (W/m^2) owing to (a) aerosols and (b) aerosols+ decrease in turbulent diffusion coefficient during the explosive growth stage.

Fig. 6. Profiles of average temperature change in Jing–Jin–Ji owing to AF (K) during 15–20 December 2016.

Fig. 7. Sounding-observed and modeled temperature profiles in EXP1 and EXP2 during the (a) climbing stage and (b) explosive growth stage in Beijing and Xingtai.

Fig. 8. Hourly change of $PM_{2.5}$_OBS, $PM_{2.5}$_EXP1, $PM_{2.5}$_EXP2, and $PM_{2.5}$_EXP3 ($\mu g/m^3$), together with the diffusion coefficient (DC) at 950 hPa of the three experiments (DC_EXP1, DC_EXP2, DC_EXP3) during 15–22 December 2016 in (a) Beijing and (b) Xingtai.

Fig. 9. Diagrammatic sketch of the contributions of AF and decrease in turbulent diffusion coefficient (DTD) to the $PM_{2.5}$ explosive growth.

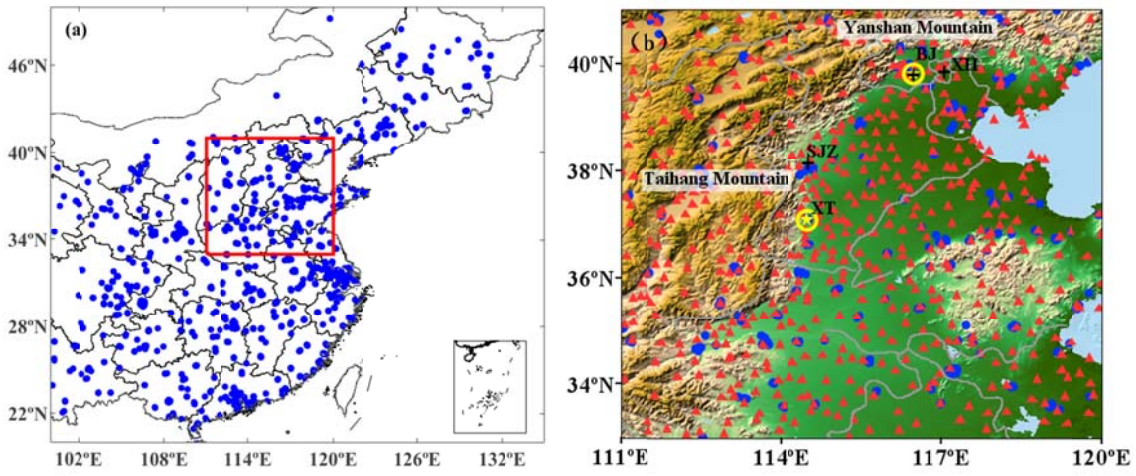

774

774 **Fig. 1.** (a) Model domain and location of Jing–Jin–Ji. (b) Geographic location and topography of Jing–Jin–
775 Ji. Blue dots are the locations of $PM_{2.5}$ observations; red triangles are the locations of automatic weather
776 stations; yellow stars are the two sounding stations; black crosses are the CARSNET and AEROSNET
777 stations.

775

776

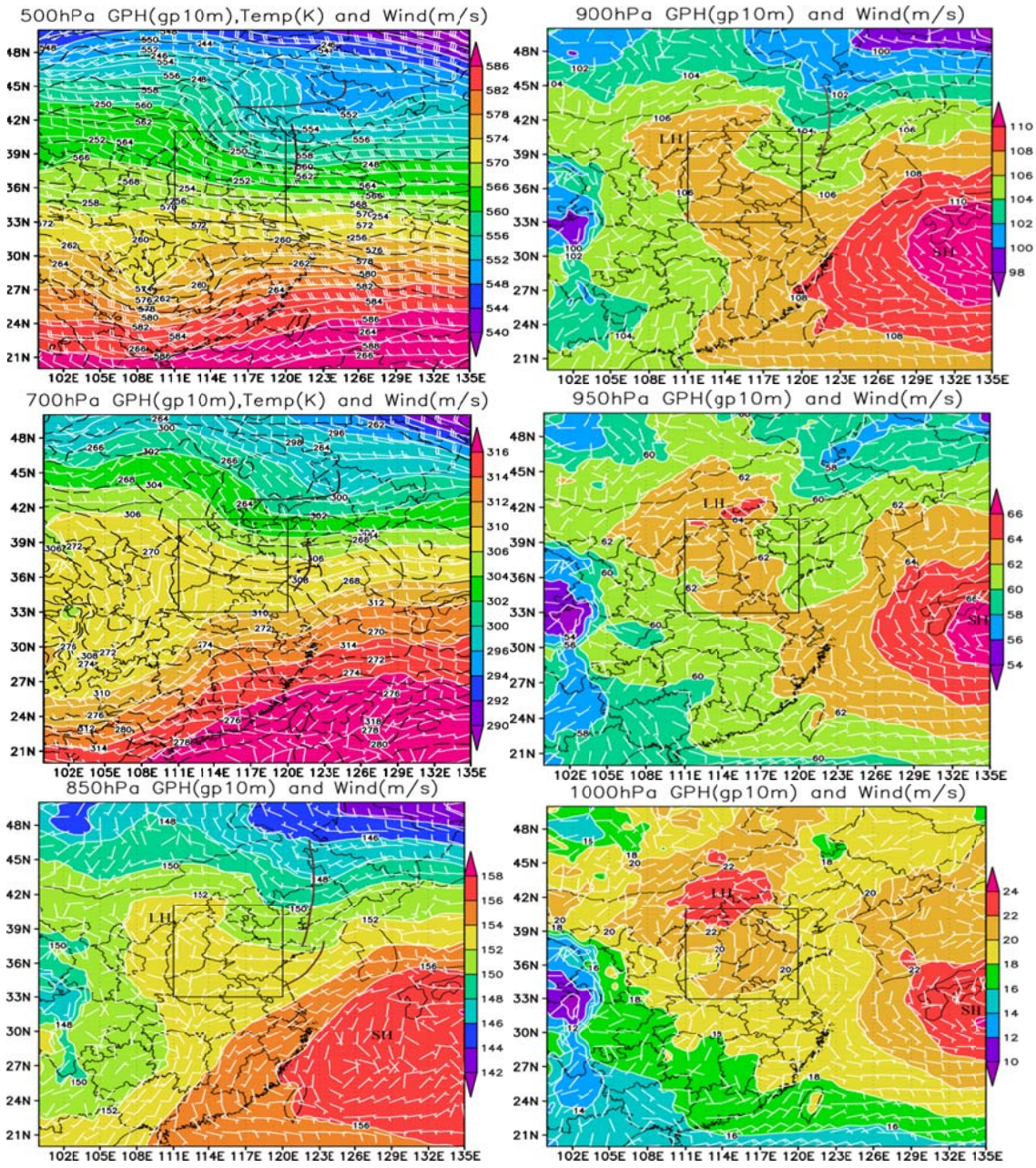

Fig. 2. Geopotential height (color-shaded; gp10m), temperature (dashed black contours; K) and wind (wind bars; m/s) in the (a) upper (500 hPa) and (b) middle (700 hPa) atmosphere, and geopotential height and wind in the (c) lower atmosphere (850 hPa) and (d–f) PBL (900, 950, 1000 hPa), at 0000 UTC 19 December 2016.

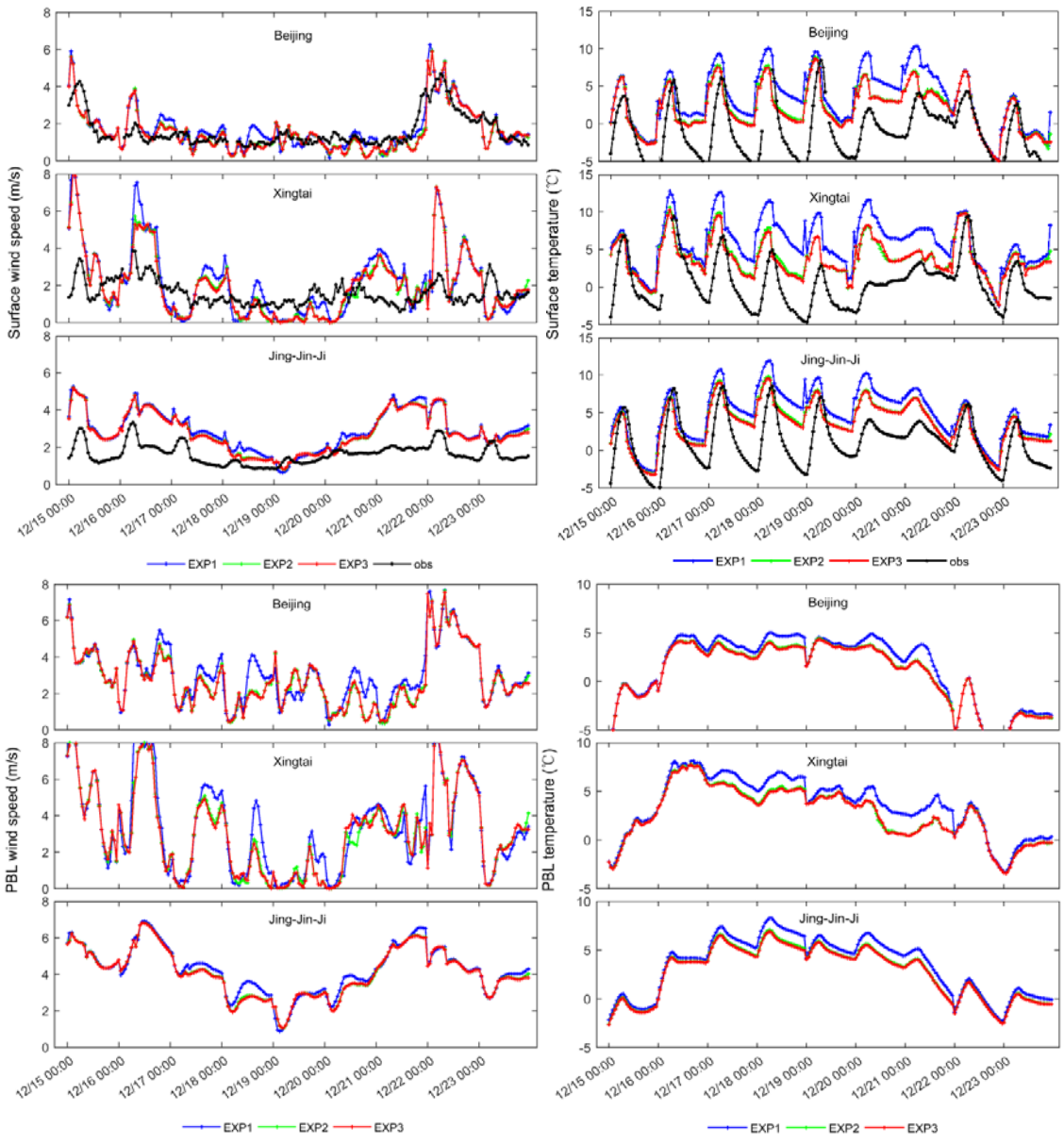

Fig. 3. Observed and modeled wind speed and temperature at the surface (upper panels), and the PBL-mean wind speed and temperature (lower panels), from the results of EXP1, EXP2 and EXP3 for Beijing, Xingtai, and the average for Jing–Jin–Ji as a whole, during 15–24 December 2016.

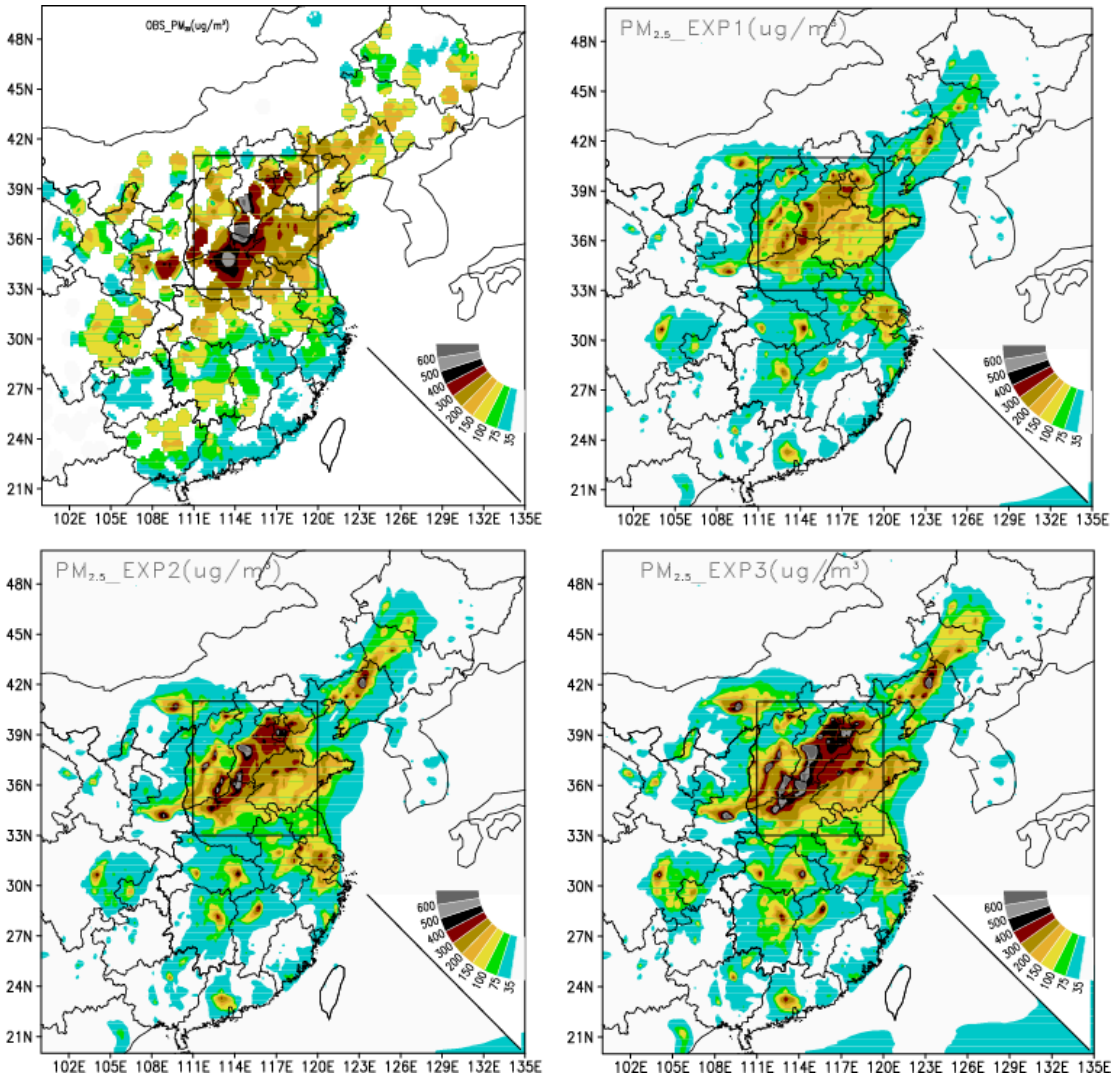

Fig. 4. Mean observed (OBS_$PM_{2.5}$) and modeled $PM_{2.5}$ concentration (μg/m^3) of the $PM_{2.5}$ explosive growth stage, from the results of EXP1, EXP2 and EXP3 ($PM_{2.5}$_EXP1, $PM_{2.5}$_EXP2 and $PM_{2.5}$_ EXP3, respectively).

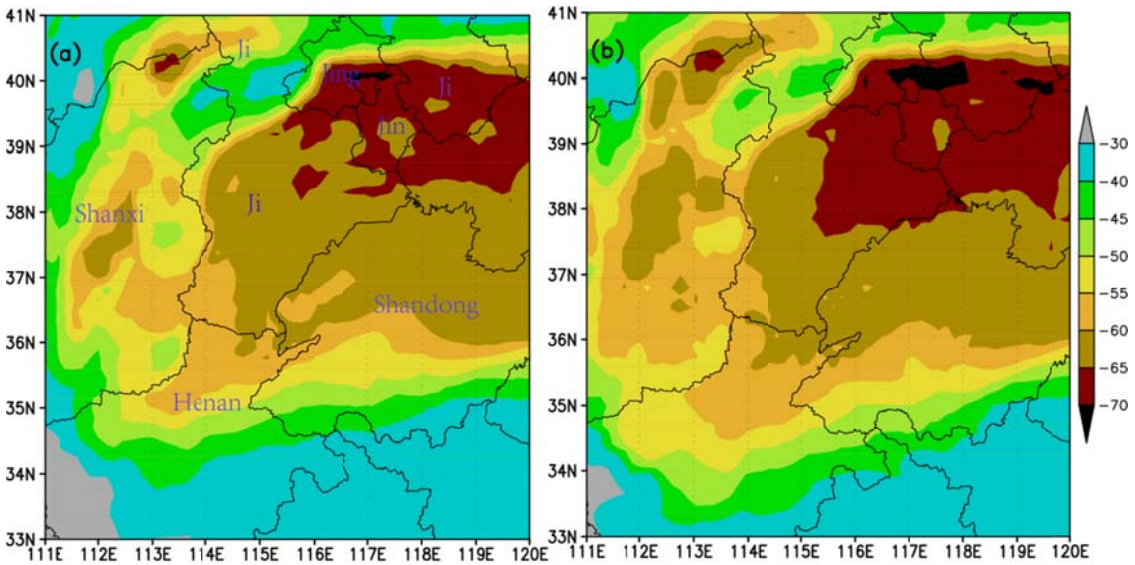

Fig. 5. Mean percentage change in SDSRF (W/m^2) owing to (a) aerosols and (b) aerosols+ decrease in turbulent diffusion coefficient during the explosive growth stage.

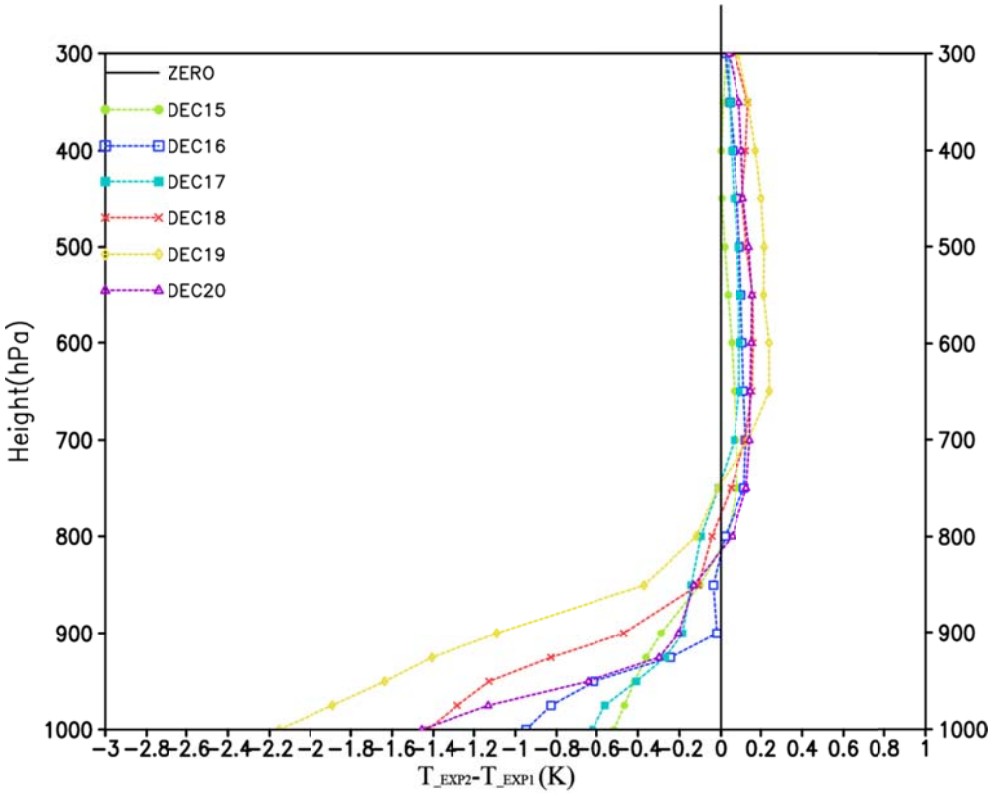

Fig. 6. Profiles of average temperature change in Jing–Jin–Ji owing to AF (K) during 15–20 December 2016.

929

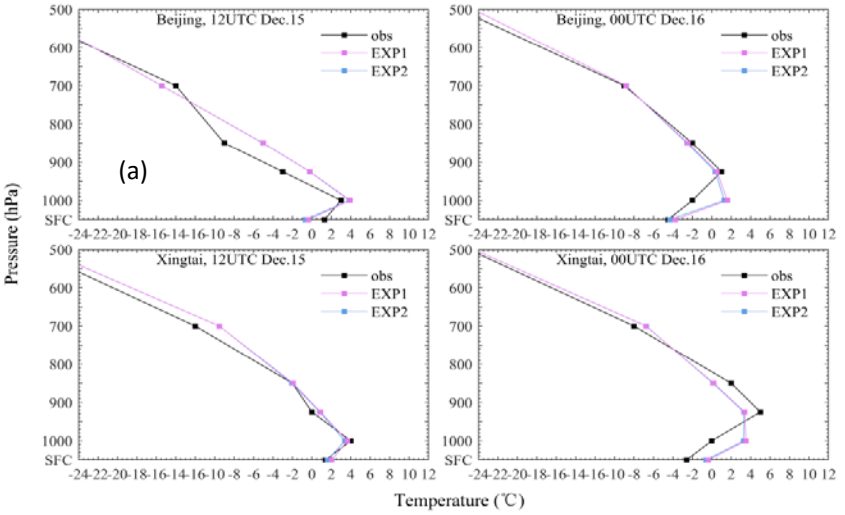

930

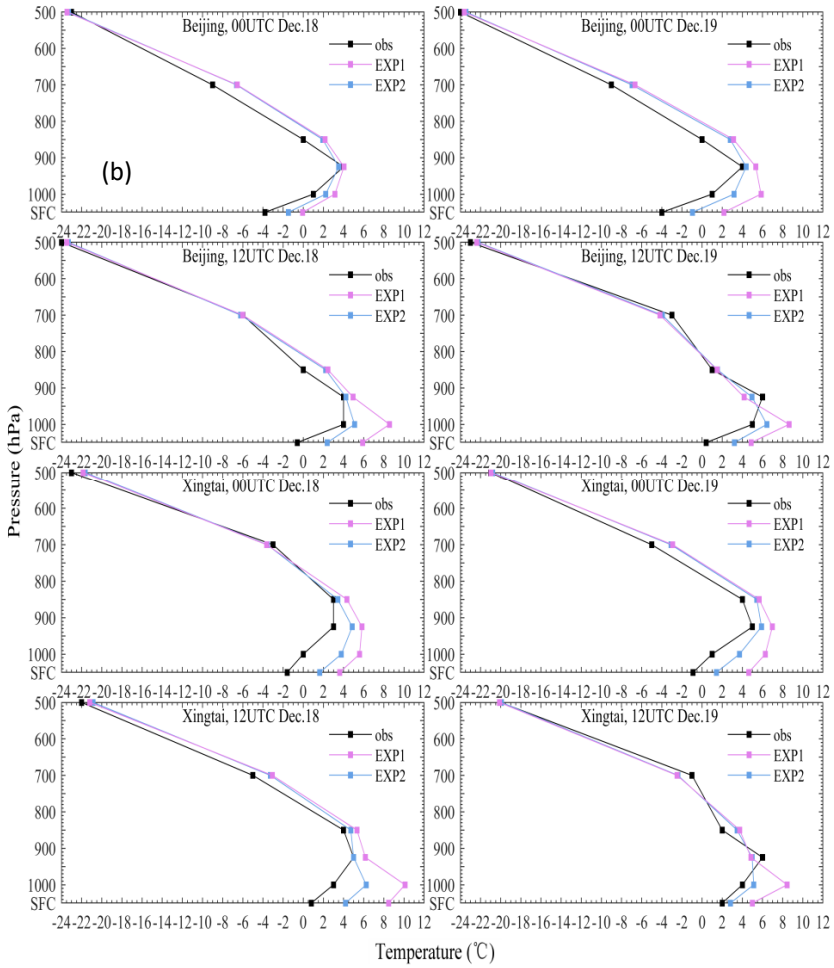

931 **Fig. 7.** Sounding-observed and modeled temperature profiles in EXP1 and EXP2 during the (a) climbing

932 stage and (b) explosive growth stage in Beijing and Xingtai.

933

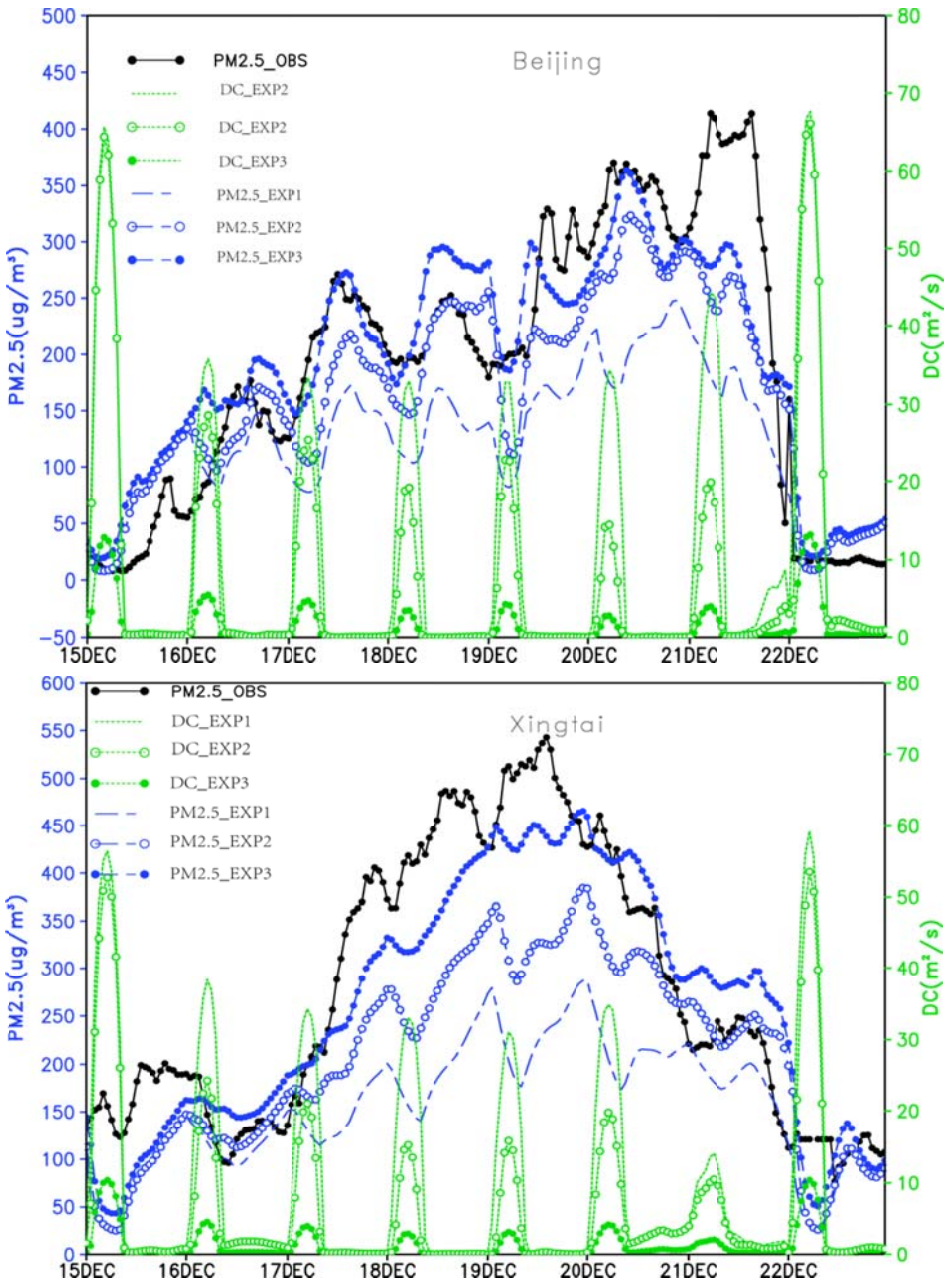

Fig. 8. Hourly change of $PM_{2.5}$_OBS, $PM_{2.5}$_EXP1, $PM_{2.5}$_EXP2, and $PM_{2.5}$_EXP3 (μg/m^3), together with the diffusion coefficient (DC) at 950 hPa of the three experiments (DC_EXP1, DC_EXP2, DC_EXP3) during 15–22 December 2016 in (a) Beijing and (b) Xingtai.

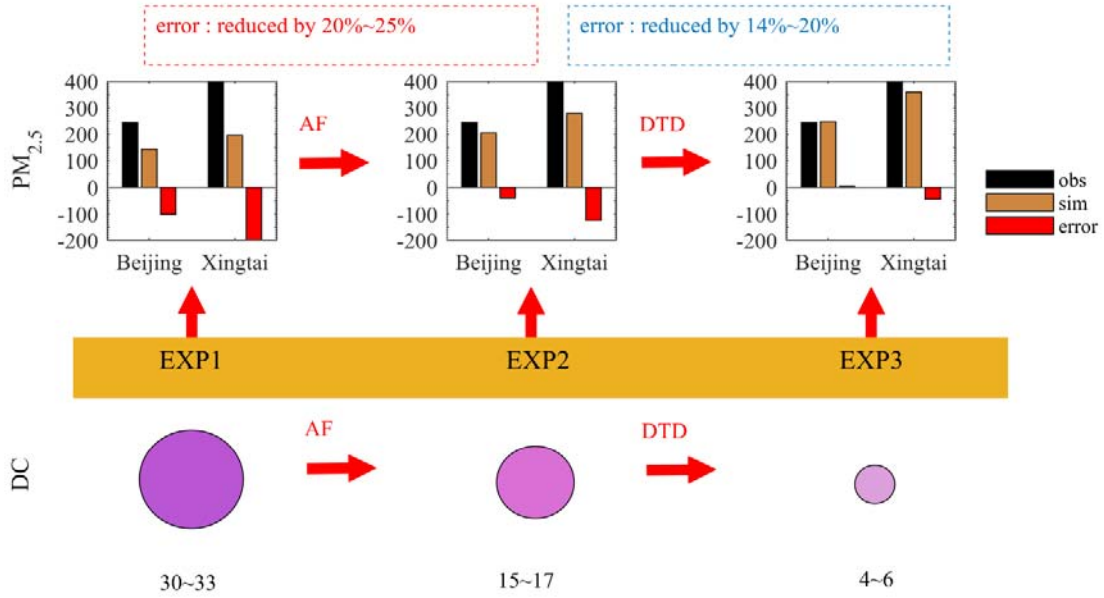

Fig. 9. Diagrammatic sketch of the contributions of AF and decrease in turbulent diffusion coefficient (DTD) to the $PM_{2.5}$ explosive growth.